Article

Construction of sp2/sp3 Hybrid Carbon Thin Layers on Silicon Substrates Using Nonequilibrium Excitation Reaction Fields

Norihiro Shimoi*

Cite This: *ACS Omega* 2023, 8, 39673−39679

Read Online

ACCESS | 📊 Metrics & More | 📰 Article Recommendations

ABSTRACT: The authors have developed a crystal growth process that utilizes electron beams from field emission (FE) to grow materials bottom-up by a method other than the transfer of thermal energy. In this study, highly crystalline single-walled carbon nanotubes were used as a field emission electron source. Electron beams with high resolution energy emitted from the source were irradiated onto acetylene gas as a nonequilibrium reaction field to induce acetylene dissociation. The generated carbon ions were then irradiated onto a [100] silicon substrate, resulting in the irradiation of the silicon substrate surface with graphene. Moreover, the crystal growth of sp2/sp3 hybrid carbon thin layers, which is different from the crystal structures of graphite, diamond, and diamond-like carbon, proceeded on the surface of the silicon substrate. Carbon layers on periodic crystal structures whose growth depends at least on the morphology of the substrate are formed through bridging with the binding site of the substrate. The authors have succeeded in developing a nonthermal technique of crystal bridging between different elements. The substrate on which the carbon layer is formed is not limited to silicon; other substrates with various crystal structures and periodicities are expected to be used.
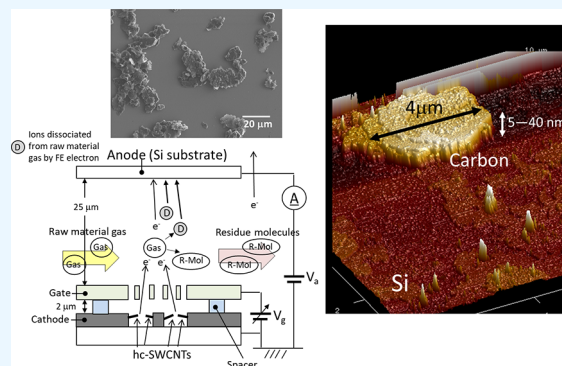
1. INTRODUCTION

In the material formation process, general chemical reaction processes involving bonding and dissociation between atoms and molecules, with or without catalysts, are generally accompanied by heating and waste heat treatment. Regardless of whether the material is solid, liquid, or gas, the heat exchange that occurs in the reaction processes of these materials requires processes to maintain the reaction field, namely, heating, heat retention, and cooling.

The authors are conducting research on bottom-up material formation processes utilizing reaction fields such as electron beams, plasma, and high-power lasers as a method of exchanging reaction energy by processes other than heating. These reaction fields are called nonequilibrium excitation reaction fields, and the process of bonding between metals and other heterogeneous materials using these reaction fields has already been reported[1−3] and used to fabricate highly functional materials. Using a nonequilibrium excitation reaction field, the author synthesized compounds from semiconductor and carbon materials that are not silicon carbide (SiC). To the best of our knowledge, no research group has reported on the synthesis of composites comprising silicon and carbon.

The nonequilibrium excitation reaction field employed in this study is a reaction field in which atoms and molecules comprising a solid can be induced and manipulated by irradiating them with a focused electron beam or ions with an acceleration energy on the keV order.[4,5] In the reaction field, a bottom-up specific reaction is induced by excitation processes and the activation using binding energy at atomic and molecular scales, for which various nano- and microstructures with heteroelements have been studied.[6,7] In this study, the author fabricated composite grains on a silicon substrate using ions or radicals of carbon atoms generated by the dissociation of organic molecules irradiated with a field-emission (FE) electron beam[8−10] in a nonequilibrium excitation reaction field on the basis of our previous study.[11] Moreover, the authors examined a technique of controlling the atomic arrangement by crystal bridging between silicon and carbon to develop composite layers.

The synthetic interfacial bonding between dissimilar elements, including metals, ceramics, and plastics, has markedly affected the properties of various composite materials. For example, metal−ceramic composite layers,[12−14] plastic−metal thin film composites,[15−17] electronic device materials,[18−20] and

heat-insulating ceramic coatings[21−23] are fabricated utilizing metal and ceramic bonding processes. In these composite materials, it is necessary to analyze the chemical bonding states and crystal structures of the interfaces between heteroelements with widely different chemical bonding states and to clarify their correlation with physical properties.

In this study, the aim is to attempt to fabricate a new crystallographic layer of a carbon material employing a nonequilibrium excitation field. The author fabricates a carbon thin layer on a silicon substrate, which is considered to be different from the crystal structures of graphene composites,[24−27] SiC,[28,29] diamond,[30,31] diamond-like carbon,[32,33] and others. In this study, the author will describe the results of our study with regard to the crystal structure, chemical bonding, and electronic structure of the silicon−carbon interface.

2. EXPERIMENTAL SECTION

In this study, the author used FE electron beams as a nonequilibrium excitation reaction field. FE electron beams are based on quantum mechanical electron tunneling with the Fowler−Nordheim model, and the energy distribution of FE electrons can be narrower than that of thermal electrons. It is also possible to efficiently emit a large number of electrons at a low voltage.[34] To obtain a stable electron emission and arbitrarily manipulate the electron emission to mA order in a low vacuum,[11,35] the author used carbon nanotubes, particularly highly crystalline single-walled carbon nanotubes (hc-SWCNTs), as an electron source.[11] The author constructed a nonequilibrium excited reaction field apparatus by adding hc-SWCNTs into indium−tin oxide (ITO) conductive thin films to form a planar FE source.

Figure 1(a) shows the configuration of the apparatus. The chamber in Figure 1(a) has a gas insert line and a gauge to monitor the vacuum. The pressure of a vacuum in a chamber maintaining a gas at approximately 1.0 Pa is controlled by adjusting the gas injection pressure and the main valve for differential pumping. The device in Figure 1(a) consists of a planar electron source doped with hc-SWCNTs as field emitters, a counter electrode with a [100] crystallographic orientation silicon substrate at a voltage of 100 V without heating treatment, and a multistage gate electrode, which was fixed at 2 μm floating from the cathode surface with glass spacers formed by printing, between the electrodes to control and increase the amount of electron emission. A carbon-based gas (acetylene was used in this study) flows near the gate electrode of the reaction system, as shown in Figure 1(a). The acetylene induces collision and dissociation reactions with the electron beam emitted from the hc-SWCNTs. The carbon ions and electron beams generated by the dissociation reaction are accelerated and collide with the silicon substrate on a counter electrode, depositing a carbon layer on the silicon substrate. Figure 1(b) shows the FE characteristics of the planar electron source with hc-SWCNTs at 1.0 Pa in an acetylene atmosphere, where the electron emission of about 0.14 mA/cm^2 was successfully controlled at a voltage of approximately 10 V on the gate electrode. The inset in Figure 1(b) shows the planar emission image obtained when the anode electrode is replaced from a silicon substrate to a low-voltage fluorescent film. The silicon substrates used in this experiment were treated with hydrofluoric acid to remove any natural oxide film, and the treated substrates used as an anode electrode were stored in a vacuum to prevent exposure to the atmosphere. The substrates were transferred to the reaction system by using a transfer vessel chamber.
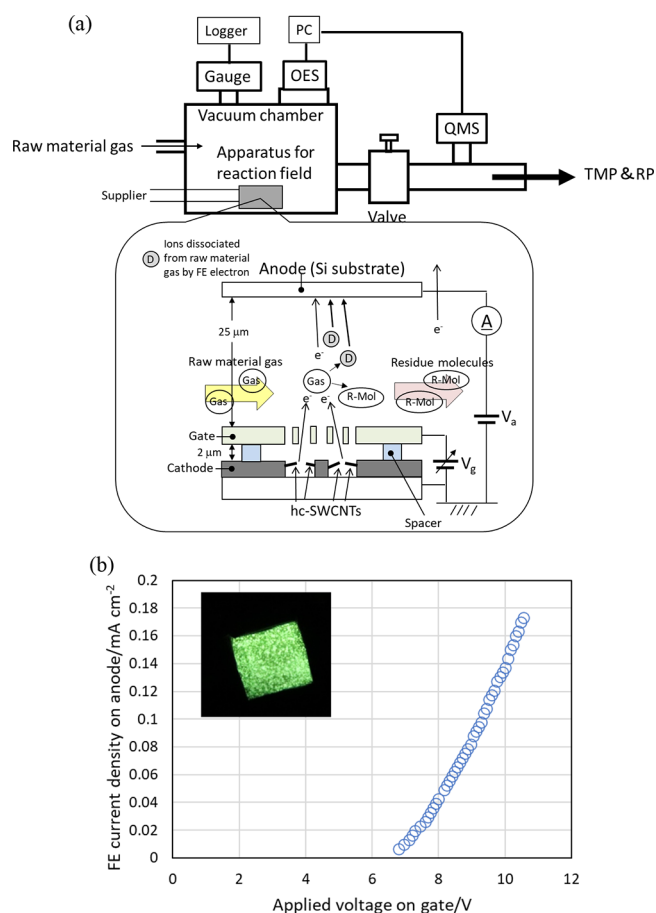
Figure 1. (a) Schematic of the nonequilibrium excited reaction field system using hc-SWCNTs. (b) Current−voltage (I−V) curve of hc-SWCNTs at 1.0 Pa in an acetylene atmosphere used for FE. The inset shows the planar emission image of the fluorescent film biased at 100 V.

The exposure conditions used are listed in Table 1. The acceleration voltage (V_a) of the ion group produced by the

Table 1. Exposure Conditions for Nonequilibrium Excitation Reaction Field

cathode electrode size	10×10 mm^2
supplied voltage on gate (V_g)	10 V
FE current density (dose)	0.14 mA/cm^2 (10^{19} electrons/cm^2)
acceleration voltage (V_a)	100 V
acetylene partial pressure (vacuum)	1.0 Pa

dissociation of acetylene and the FE electron beam was set to 100 V. The presence or absence of carbon film formation and crystallinity varies with the amount of charge and the acceleration voltage corresponding to the energy of the electron beam. Therefore, the author focuses on the formation conditions under which crystalline films were observed and analyses of the crystalline films produced are reported in this study.

3. RESULTS AND DISCUSSION

The hc-SWCNTs are expected to serve as field emitters that can emit electrons stably in a vacuum greater than approximately 1.0 Pa with acetylene, regardless of the type of active or inert gas used. Figure 2(a)−(d) shows the partial pressure in the chamber illustrated in Figure 1(a) to measure the correlations of the FE
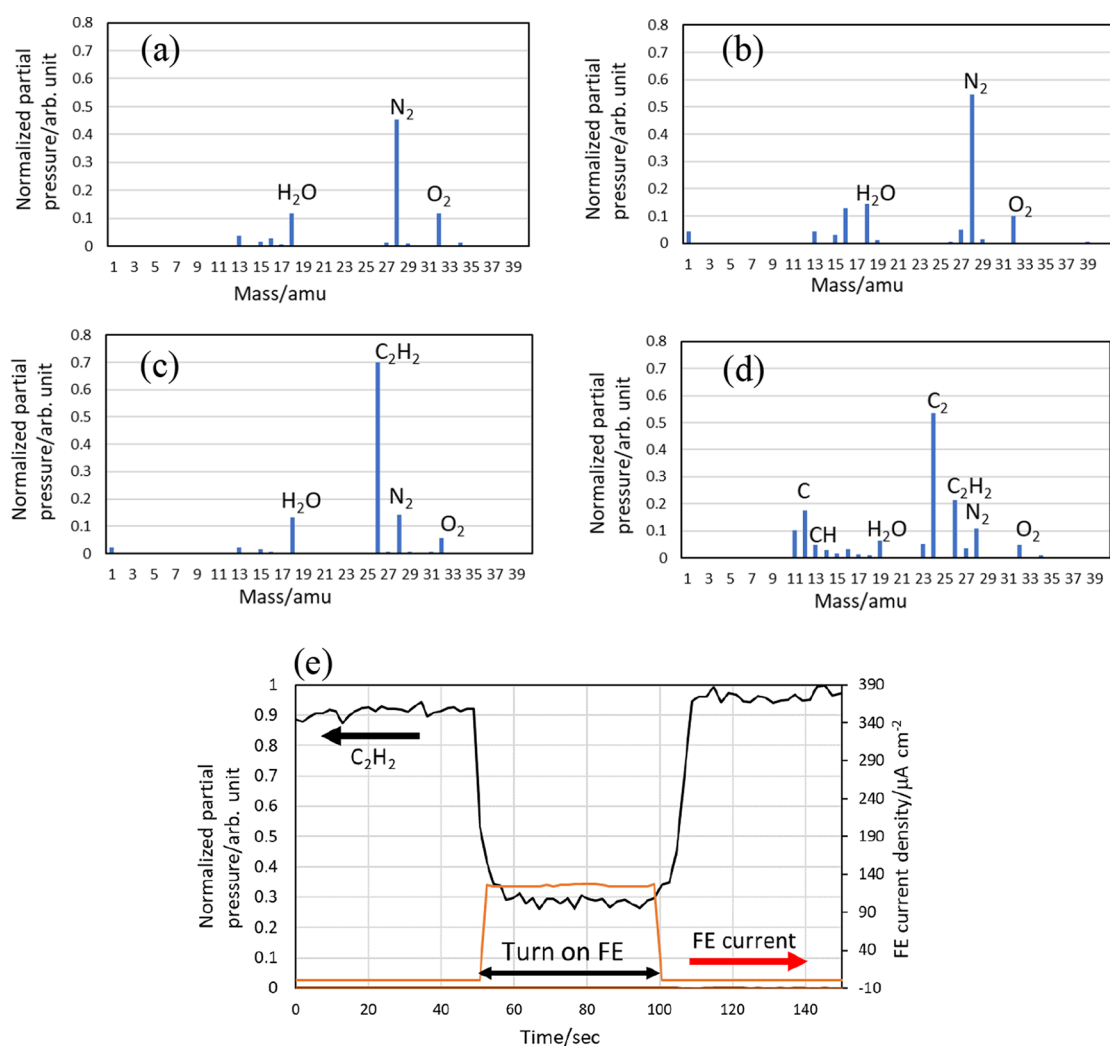
Figure 2. Correlation of FE current with decompression by acetylene dissociation in a QMS. (a) Vacuum without field emission irradiation. (b) Vacuum with field emission irradiation. (c) Without field emission irradiation with acetylene gas injection. (d) Injected with acetylene gas and irradiated with field emission beams. (e) Acetylene gas partial pressure due to on−off FE radiation.

current with decompression by acetylene dissociation in a quadrupole mass spectrometer (QMS; Cannon Anelva Corporation). The author succeeded in confirming the phenomenon of the dissociation of acetylene gas induced by FE electron beams after its introduction to the chamber. Furthermore, the partial pressure of acetylene shown in Figure 2(e) was also measured using a QMS. It was found that the on−off of FE electron beams and the change in the partial pressure of acetylene were synchronized. This finding indicates that the gas is dissociated by the interaction between the gas molecules and electrons as the electrons pass through the acetylene atmosphere. Making use of the acetylene dissociation induced by FE electron beams, the authors irradiated silicon substrates with electron beams and carbon or hydrocarbon ions that were generated by acetylene dissociation. In addition, the dissociation of acetylene gas produced under the conditions in Table 1 was also observed as luminescence using an optical emission spectrometer (OES; Ocean Insight inc.) from outside the chamber. The results are shown in Figure 3. The spectrum is consistent with the dissociation spectrum of acetylene plasma, and the dissociation of C_2 and CH was confirmed from the spectrum at around 400 nm.
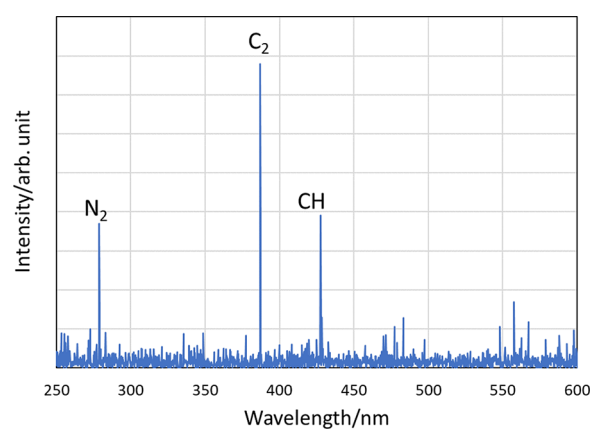
Figure 3. Optical emission spectroscopy inside the chamber with the conditions shown in Table 1.

A scanning electron microscopy (SEM) image of the deposits on the silicon substrate synthesized under the conditions listed in Table 1 is shown in Figure 4(a). It was observed that the deposits were distributed nonuniformly on the silicon substrate to form grains or thin layers. Figure 4(b) shows a magnified
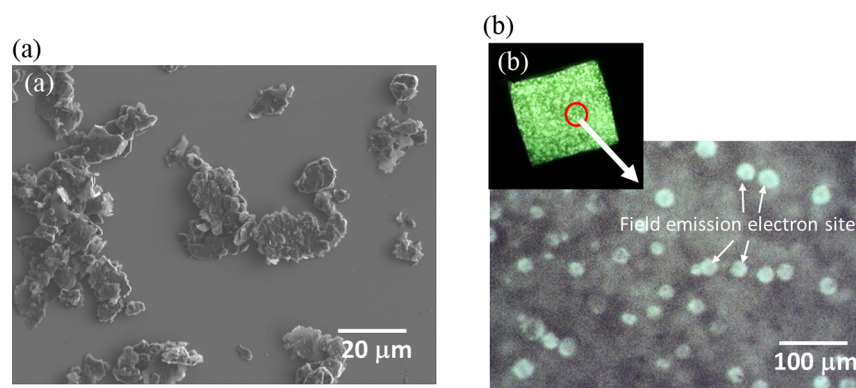
Figure 4. (a) SEM image of grainlike deposits forming a thin layer on a silicon substrate. (b) Magnified image of FE electron site distribution extracted from the area encircled in red in the planar luminescence photograph in the inset of Figure 1(b). Bright spots show FE electron sites.
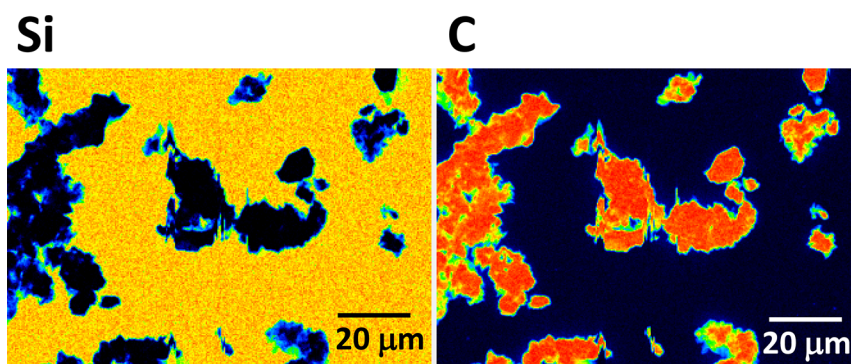
Figure 5. Images of grain thin layers deposited on silicon substrates obtained using EPMA. The left figure shows the elemental mapping of silicon atoms, and the right figure shows the elemental mapping of carbon atoms. The measurement area is the same as that in Figure 4(a).
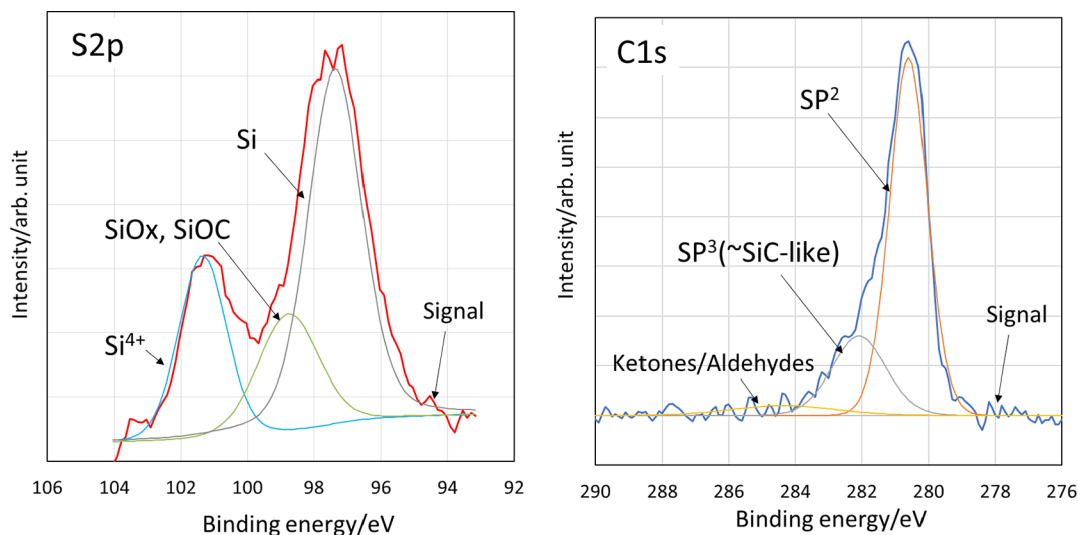
Figure 6. X-ray photoelectron spectra derived from silicon and carbon in a carbon thin layer.

image of the bright spot distribution on the FE surface for reference. The distribution of the FE electron sites is similar to that of the deposits in Figure 4(a). The composition of these deposits was analyzed using an electron probe micro analyzer (EPMA; JEOL), as shown in Figure 5. The deposits on the silicon substrate were found to consist of carbon. The authors confirmed the dissociation of acetylene gas induced by the FE electron beams, as shown in Figures 3 and 4. It is guessed that the deposits on the silicon substrate are formed from the reaction of acetylene gas with FE electron beams.

Figure 6 shows the X-ray photoelectron spectroscopy (XPS; Bruker) spectra of the state of bonding silicon and carbon in the carbon grain layer on the silicon substrate shown in Figure 4. The spectrum of sp2 in Figure 6 derived from SiC with a peak around the binding energy of 100 eV was hardly developed. Furthermore, the signals derived from silicon atoms and SiOC or SiOx (Si^{3+}) were identified. The Si^{4+} signal is assumed to indicate an oxidation state derived from SiO_2. As for C 1s of carbon in Figure 6, it was found that the carbon thin layer has tetrahedral carbon bonding states originating from diamond or

SiC structures with electronic states related to sp3 orbitals. The crystal structure depends on the dangling bonds and periodic crystal structure of silicon atoms on the surface of a silicon substrate on which the carbon thin layer is formed, and the layer is assumed to have a crystal structure similar to a mixed-crystal structure of graphite layers and tetrahedral structures such as SiC.[13,14]

Figure 7 shows a scanning probe microscopy (SPM; Bruker) image of the morphology of a carbon grain thin layer on a silicon
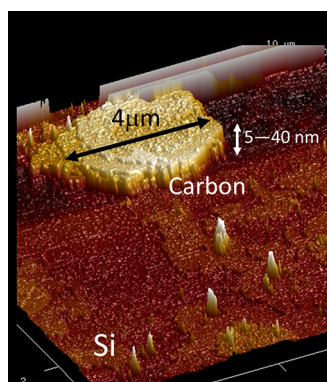
Figure 7. SPM image of surface topography of the carbon thin layer synthesized on a silicon substrate.

substrate. The electron beam and acetylene-dissociated ions with an energy of 100 eV, which depends on the acceleration voltage of 100 V, were irradiated and deposited on a silicon substrate as the counterelectrode. Figure 7 shows the $I-V$ characteristics obtained when a voltage is applied between the probe and the substrate in SPM. The conductivity of the carbon grain thin layer and the silicon substrate was measured with the time of exposure of a silicon substrate to FE electron beams and carbonaceous ions controlled to 40 and 120 s by using the nonequilibrium excitation reaction field shown in Figure 1. As a reference, the conductivity in the bulk direction was also measured for a thin film of 10 layers of graphene sheets on a silicon substrate and a 100 nm-thick aluminum thin film deposited by sputtering. The SPM cantilever used in this study was copper, and an irreversible $I-V$ curve was observed using to the Schottky contact with the silicon substrate. The highest conductivity in the bulk direction was observed for the carbon thin layer deposited in a nonequilibrium excited reaction field for 120 s. The current flow was 20 times more conductive than that in the stacked graphene and aluminum films on a silicon substrate. The $I-V$ curves of the carbon layer with 120 s exposure to the acetylene-dissociated ions, which are independent of the polarity of the applied voltage, suggest the occurrence of electrically conducting and crystal bridging between the silicon substrate and the carbon thin layer.

The carbon sample was sliced by using a focused ion beam (FIB). High-resolution transmission electron microscopy (HRTEM; JEOL Ltd.) with an acceleration voltage of 300 kV was carried out to obtain detailed information about the crystal structure near the interface between the silicon substrate and the carbon thin layer. Figure 8 shows an HRTEM image of the interface between the silicon substrate and the carbon layer. It shows that a crystallized carbon layer of approximately 5 nm thickness was synthesized on the silicon substrate surface and a clear interface between the silicon substrate and the carbon layer was formed. These diffraction images show a pattern related to
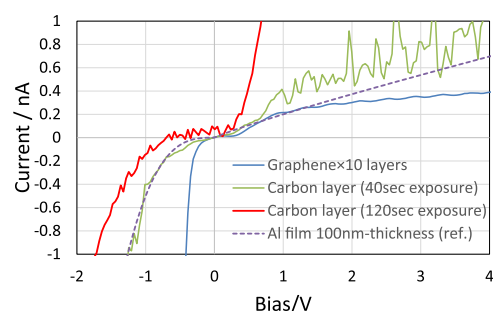
Figure 8. $I-V$ curves of carbon and reference thin layers synthesized on silicon substrates analyzed by using SPM cantilevers as probes.

the [100] alignment of silicon. From the inset images in Figure 9(a), it is confirmed that the carbon film has a structure different
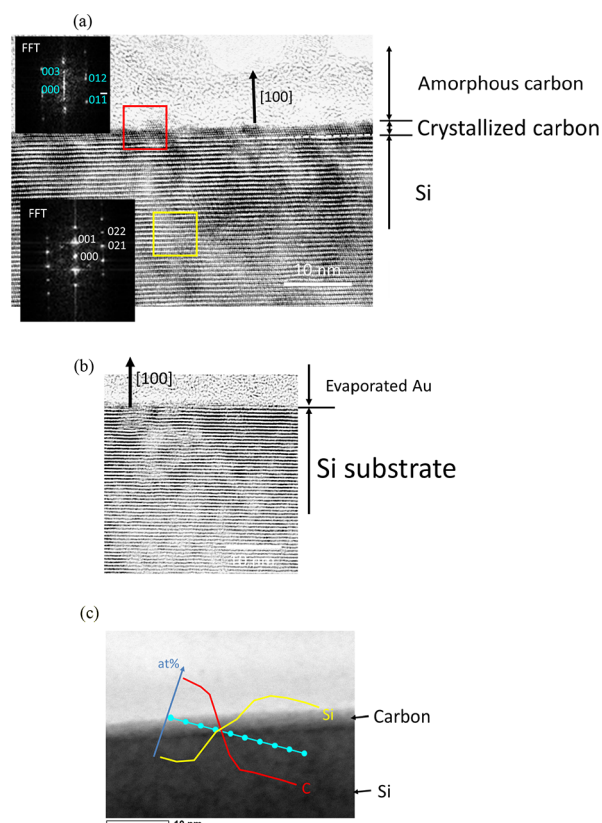
Figure 9. (a) (Entire) HRTEM image of silicon−carbon thin layer near the surface of silicon substrate. (Red frame) Fourier transform image of diffraction near the carbon thin layer. (Yellow frame) Fourier transform image of the bulk of silicon substrate. (b) Surface of silicon substrate without carbon deposition as a reference. (c) Atomic distribution of carbon (Red line) and Si (Yellow line) by EDS in HRTEM.

from the crystal structures of graphite, graphene on SiC, and diamond, and from the conventional bulk in the silicon substrate. Moreover, a crystalline interface is formed. On the other hand, the surface of the silicon substrate was exposed in the areas where no deposits existed, as shown in Figure 9(b), and it was confirmed that no other crystal structures were formed. The top of the layer consisted of amorphous Au deposited by evaporation. Figure 9(c) shows atomic distribution of silicon and carbon as measured by energy-dispersive X-ray spectroscopy (EDS) in HRTEM. The atomic concentration expressed as atomic percentage (at %) of each atom is indicated for each

measurement point, and it was found that atomic concentration was clearly different at the interface between the silicon substrate and the carbon layer.

The carbon layer synthesized on the silicon substrate in this study showed a structure different from that of graphite. It is assumed that the acetylene dissociation induced by FE electron irradiation and the presence of carbonaceous ions formed after dissociation contribute to the formation of the carbon thin layer. In particular, the crystal structure of the carbon layer synthesized on the silicon substrate shows a diffraction pattern different from that reported for SiC formed by epitaxial growth on the silicon substrate.[13]

From the above results, the carbon layer synthesized near the silicon surface is expected to have a continuous crystal structure composition different from those of graphite layers and diamonds. It is assumed that the crystal structure is formed depending on the dangling bonds and periodic crystal structure on the substrate side where the carbon layer is constructed.[10] The above analysis confirms the existence of dangling bonds of silicon and crystal bridging of carbon. Moreover, the carbon layer shown in Figure 8 has a crystalline structure different from those of graphite, graphene, diamond, and diamond-like carbon.

4. CONCLUSIONS

The authors have found that a carbon thin layer is formed on the surface of a silicon substrate by irradiating a group of carbonaceous ions and electron beams accelerated on the kV order onto the silicon substrate as a nonequilibrium excited reaction field after the dissociation of acetylene with FE electron beams using hc-SWCNTs. The crystal structure of the carbon layer is different from those of graphite, graphene, diamond, and diamond-like carbon, and it is assumed to depend on the periodic crystal structure of the substrate on which the crystal is grown.[36]

In this study, the carbon layer was inferred to have a crystal-bridged structure on the face orientation [100] of the silicon substrate. Furthermore, the carbon layer was composed only of pure carbon, which depends on the crystal structure of the substrate without the intercalation of different elements in the graphite layer. In this study, the authors formed sp2/sp3 hybrid carbon thin layers using silicon substrates with a plane orientation of [100]. The author also formed carbon thin layers by controlling the acceleration energy of electron beams and carbonaceous ion groups in order to achieve crystal bridging between ceramics and carbon films, not only between metals and semiconductors.[10] The possibility of forming a periodic crystal structure of only carbon, which is different from those of graphite, graphene, diamond, and diamond-like carbon, is expected by controlling the acceleration energies of electron beams and groups of carbonaceous ions. In the future, we will attempt to synthesize composite materials with carbon on substrates with various crystal structures and start synthesizing composite materials with high functional electrical, physical, and chemical properties. The method of forming a uniform carbon film with a nanoscale thickness while ensuring conductivity is the first of its kind in the world and is considered highly applicable as a conductive coating material.

ASSOCIATED CONTENT

Data Availability Statement

The data that support the findings of this study are available within the article.

AUTHOR INFORMATION

Corresponding Author

Norihiro Shimoi − *Department of Electrical and Electric Engineering, Tohoku Institute of Technology, Sendai, Miyagi 982-8577, Japan;* ● orcid.org/0000-0002-3787-3767; Email: n-shimoi@tohtech.ac.jp

Complete contact information is available at:
https://pubs.acs.org/10.1021/acsomega.3c05608

Notes

The author has declared that no competing financial or nonfinancial interests existed at the time of publication.
The author declares no competing financial interest.

REFERENCES

(1) Alexabder, B. H.; Balluffi, R. W. The mechanism of sintering of copper. *Acta Metall.* **1957**, 5 (11), 666−677.

(2) Ardell, A. J. Effect of volume fraction on particle coarsening - theoretical considerations. *Acta Metall.* **1972**, 20 (1), 61.

(3) Bae, S. I.; Baik, S. Determination of critical concentrations of silica and/or calcia for abnormal grain growth in alumina. *J. Am. Ceram. Soc.* **1993**, 76 (4), 1065−1067.

(4) David, S. A.; Babu, S. S.; Vitek, J. M. Welding: Solidification and microstructure. *JOM* **2003**, 55 (6), 14−20.

(5) Locke, B. R.; Shih, K. Y. Review of the methods to form hydrogen peroxide in electrical discharge plasma with liquid water. *Plasma Sources Sci. Technol.* **2011**, 20 (3), No. 034006.

(6) Yilbas, B. S. Entropy analysis in an Au-Cr two-layer assembly during laser shortpulse heating. *Numer. Heat Transfer, Part A* **2003**, 43 (2), 179−199.

(7) Edmondson, P. D.; Young, N. P.; Parish, C. M.; Moll, S.; Namavar, F.; Weber, W. J.; Zhang, Y. W. Ion-beam-induced chemical mixing at a nanocrystalline CeO$_2$-Si interface. *J. Am. Ceram. Soc.* **2013**, 96 (5), 1666−1672.

(8) Fujimura, T.; Tanaka, S.-I. In-Situ High temperature X-ray diffraction study of Cu/Al$_2$O$_3$ interface reactions. *Acta mater.* **1998**, 46 (9), 3057−3061.

(9) Cheng, B.-C.; Yu, X.-M.; Liu, H.-J.; Fang, M.; Zhang, L.-D. Enhanced effect of electron-hole plasma emission in Dy, Li codoped ZnO nanostructures. *J. Appl. Phys.* **2009**, 105 (1), No. 014311.

(10) Shimoi, N.; Tanaka, S.-I. Nonthermal crystal bridging of ZnO nanoparticles by nonequilibrium excitation reaction of electrons and plasma without cross-linking agent on plastic substrate. *J. Alloys Compd.* **2019**, 797, 676−683.

(11) Shimoi, N.; Tohji, K. Field-emission durability employing highly crystalline single-walled carbon nanotubes in a low vacuum with activated gas. *J. Phys. D: Appl. Phys.* **2019**, 52 (50), 505303.

(12) Eustathopoulos, N. Dynamics of wetting in reactive metal ceramic systems. *Acta mater.* **1998**, 46 (7), 2319−2327.

(13) Iwamoto, C.; Tanaka, S.-I. Interface nanostructure of brazed silicon nitride. *J. Am. Ceram. Soc.* **1998**, 81 (2), 363−368.

(14) Rado, C.; Drevet, B.; Eustathopoulos, N. The role of compound formation in reactive wetting: The Cu/SiC system. *Acta Mater.* **2000**, 48 (18−19), 4483−4491.

(15) Liu, F. C.; Liao, J.; Nakata, K. Joining of metal to plastic using friction lap welding. *Mater. Des.* **2014**, 54, 236−244.

(16) Kang, H.; Jung, S.; Jeong, S.; Kim, G.; Lee, K. Polymer-metal hybrid transparent electrodes for flexible electronics. *Nat. Commun.* **2015**, *6*, 6503.

(17) Lee, Y.; Jin, W.-Y.; Cho, K. Y.; Kang, J.-W.; Kim, J. Thermal pressing of a metal-grid transparent electrode into a plastic substrate for flexible electronic devices. *J. Mater. Chem. C* **2016**, *4*, 7577−7583.

(18) Llorca, J.; Needleman, A.; Suresh, S. An analysis of the effects of matrix void growth on deformation and ductility in metal ceramic composites. *Acta Metall. Mater.* **1991**, *39* (10), 2317−2335.

(19) Miotello, A.; Kelly, R.; Laidani, N. Chemical and compositional changes induced by ion implantation in SiC and resulting hydrogen permeation properties. *Surf. Coat. Technol.* **1996**, *65* (1−3), 45−56.

(20) Santos, M.; Filipe, E. C.; Michael, P. L.; Hung, J.-C.; Wise, S. G.; Bilek, M. M. M. Mechanically robust plasma-activated interfaces optimized for vascular stent applications. *ACS Appl. Mater. Interfaces* **2016**, *8* (15), 9635−9650.

(21) Donald, I. W. Preparation, properties and chemistry of glass-ceramic-to-metal and glass-ceramic-to-metal seals and coatings. *J. Mater. Sci.* **1993**, *28* (11), 2841−2886.

(22) Kokubo, T.; Miyaji, F.; Kim, H. M.; Nakamura, T. Spontaneous formation of bonelike apatite layer on chemically treated titanium metals. *J. Am. Ceram. Soc.* **1996**, *79* (4), 1127−1129.

(23) Kim, H. M.; Miyaji, F.; Kokubo, T.; Nakamura, T. Effect of heat treatment on apatite-forming ability of Ti metal induced by alkali treatment. *J. Mater. Sci.: Mater. Med.* **1997**, *8* (6), 341−347.

(24) Geim, A. K.; Novoselov, K. S. The rise of graphene. *Nat. Mater.* **2007**, *6* (3), 183−191.

(25) Kim, K. S.; Zhao, Y.; Jang, H.; Lee, S. Y.; Kim, J. M.; Kim, K. S.; Ahn, J.-H.; Kim, P.; Choi, J.-Y.; Hong, B. H. Large-scale pattern growth of graphene films for stretchable transparent electrodes. *Nature* **2009**, *457* (7230), 706−710.

(26) Jousseaume, V.; Cuzzocrea, J.; Bernier, N.; Renard, V. T. Few graphene layers/carbon nanotube composites grown at complementary-metal-oxide-semiconductor compatible temperature. *Appl. Phys. Lett.* **2011**, *98*, 123103.

(27) Opoku, F.; Kiarii, E. M.; Govender, P. P. Nanotechnology for Water and Wastewater Treatment Using Graphene Semiconductor Composite Materials. *Env. Nanotechnol.* **2020**, *4*, 1−34.

(28) Yoshida, K. Development of silicon carbide fiber-reinforced silicon carbide matrix composites with high performance based on interfacial and microstructure control. *J. Ceram. Soc. Jpn.* **2010**, *118* (1374), 82−90.

(29) Frazer, D.; Hosemann, P.; Back, C. A.; Deck, C.; Khalifa, H. Nano/micro scale characterization of SiC/SiC composite materials. *Microsc. Microanal.* **2012**, *18* (52), 1420−1421.

(30) Moulton, B.; Zaworotko, M. J. From molecules to crystal engineering: Supramolecular isomerism and polymorphism in network solids. *Chem. Rev.* **2001**, *101* (6), 1629−1658.

(31) Balandin, A. A. Thermal properties of graphene and nano-structured carbon materials. *Nat. Mater.* **2011**, *10* (8), 569−581.

(32) Kuznetsov, V. L.; Chuvilin, A. L.; Butenko, Y. V.; Malkov, I. Y.; Titov, V. M. Onion-like carbon from ultra-disperse diamond. *Chem. Phys. Lett.* **1994**, *222* (4), 343−348.

(33) Sengupta, R.; Bhattacharya, M.; Bandyopadhyay, S.; Bhowmick, A. K. A review on the mechanical and electrical properties of graphite and modified graphite reinforced polymer composites. *Prog. Polym. Sci.* **2011**, *36* (5), 638−670.

(34) Kimoto, K. Practical aspects of monochromators developed for transmission electron microscopy. *Microscopy* **2014**, *63*, 337−344.

(35) Shimoi, N.; Sato, Y.; Tohji, K. Highly crystalline single-walled carbon nanotube field emitters: Energy-loss-free high current output and long durability with high power. *ACS Appl. Electron. Mater.* **2019**, *1*, 163−171.

(36) Shimoi, N. Nanometer-thick crystalline carbon films having a spinel structure grown on ZnO Substrates: Implications for new ceramic−carbon composition. *ACS Omega* **2020**, *5* (50), 32334−32340.